



OPEN Enhanced extreme gradient boosting based algorithm for mobility management of autonomous vehicles from sub 6 GHz to mmWave networks

Saad Ijaz Majid¹, Sohaib Ijaz Majid², Shahid Khan³✉, Salah Ud-Din Khan⁴, Haider Ali¹, Anwar Ali⁵, Neelam Gohar⁶ & Slawomir Koziel^{3,7}✉

This paper provides an accurate target cell's RSRP (received signal received power) prediction technique for cellular handovers, ensuring robust connectivity for autonomous vehicles (AVs). We propose an extreme gradient boosting (XGBoost)-based mechanism to predict channel state information (CSI) in advance prior to a cell handover request due to lower RSRP. Our test results indicate that for speeds ranging from 0 to 120 km/h, the proposed prediction technique improves the handover success rate (HSR) by up to 4%. In particular, the average achieved success rate with the proposed algorithm is 97% compared to the conventional algorithm providing only 93% success rate. The proposed solution can work for any frequency pair and wireless technology.

Keywords Channel state information (CSI), Autonomous vehicles (AVs), XGBoost, RSRP

In AVs technology, one of the key challenges is maintaining seamless connectivity with the host as an AV is continuously moving through various wireless cells. Robust connectivity helps in ensuring uninterrupted control of signaling, data, and call flow. The handovers involved in future high-speed cellular networks pose a significant challenge to network engineers, since the massive involvement of sub 6 GHz and THz frequencies limits the cell coverage to a few hundred meters only due to involved path losses, reflection, and scattering. Consequently, a larger number of cells are now required to provide cellular coverage to a certain geographic area using these high frequencies, compared to a traditional cellular network operating in MHz band.

For each host change request, a temporary window called a measurement window (MW) is generated to scan target cell bearings. Yet, each MW essentially suspends all types of cellular traffic except the mentioned scans. This temporary suspension of traffic channel due to an MW makes the AV virtually lose contact with its serving station since no information can be exchanged during the measurement period. This may cause an AV to temporarily lose precise control signaling during this period due to no information exchange. Moreover, despite of suspending cellular traffic for an MW, the handover request may or may not be successful. This paper provides a solution to avoid frequent traffic interruptions due to an MW in AV technology, thereby ensuring seamless wireless connectivity.

The traditional event-driven handover technique fails to address dynamic and rapidly changing network environment due to its dependence on MW for each handover request. For this purpose, this research work proposes a robust data-driven handover technique, i.e., predicting the success of a handover request without an MW, and thus preempting all handover requests that are likely to fail. The proposed technique significantly eliminates handover request failures and improves HSR. The Fig. 1 shows an AV trying to handover from Base

¹Department of Electronics Engineering Technology, University of Technology Nowshera, Nowshera, Pakistan.

²Senior RAN Engineer, 2Degrees, Auckland, New Zealand. ³Faculty of Electronics, Telecommunications and Informatics, Gdansk University of Technology, 80-233 Gdansk, Poland. ⁴Sustainable Energy Technologies Center, College of Engineering, King Saud University, P.O.Box 800, 11421 Riyadh, Saudi Arabia. ⁵Department of Electronic and Electrical Engineering, Faculty of Science and Engineering, Swansea University Bay Campus, Swansea, UK. ⁶Department of Computer Science, Shaheed Benazir Bhutto Women University, Peshawar 25000, Pakistan. ⁷Engineering Optimization and Modeling Center, Reykjavik University, 101 Reykjavík, Iceland. ✉email: shahid.khan@pg.edu.pl; koziel@ru.is

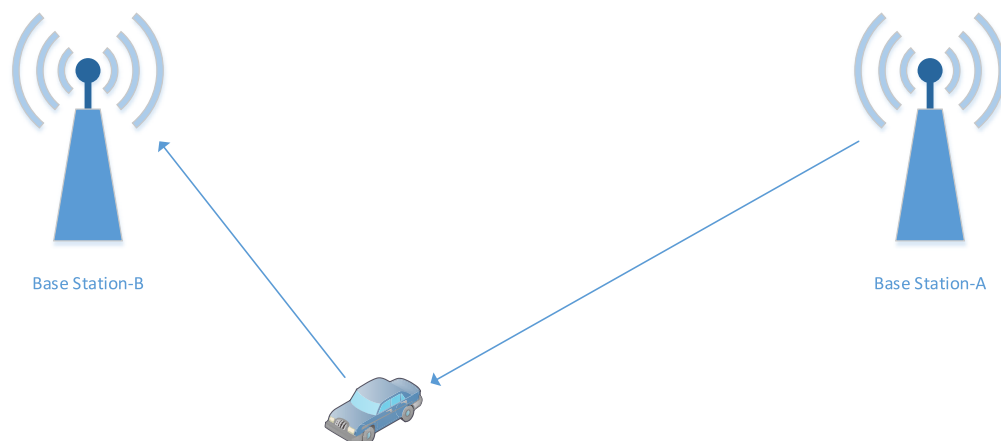


Fig. 1. An AV making handover request from base station-A to base station-B.

Station-A to Base Station-B. Now according to the conventional handover mechanism an MW gets triggered to scan for target cell bearings while temporarily suspending all the cellular traffic flow to the AV. This temporary suspension of cellular traffic flow to AV is detrimental because at this particular scan window, the AV loses its connection with the base station, while the AV might require control or data signaling for its smooth navigation. While the simulation results demonstrate promising performance, this research has certain limitations. Future work should include field-testing under real-world conditions to more accurately assess the feasibility and effectiveness of the proposed model. Additionally, further investigation is required to enhance computational efficiency and optimize the XGBoost algorithm in order to reduce processing complexity, thereby improving its suitability for deployment in autonomous vehicle (AV) systems.

In this work, we have identified the following fundamental limitations in AVs communication with the base station while using the traditional handover mechanism:

1. Event based handovers; In this case, the handover request is triggered right at the time when RSRP gets lower than the defined threshold. There is no mechanism where the AV can use already available data to predict the outcome of the upcoming handover request.
2. Frequent engagement of unnecessary MWs causing cellular traffic interruption. During this measurement period the vehicle temporarily loses its contact with the base station. Thus, no information can be exchanged during an MW.

This work provides an integrated solution to the mentioned limitations in the following manner:

1. Data-driven handovers to replace the event-based handovers. This proposed mechanism predicts the RSRP of the target cell before a handover request is even initiated by an AV.
2. Once the handover mechanism is intelligent enough to predict the success of a handover request, all potentially failing handover requests are preempted and correspondingly all unnecessary MWs are avoided.

Literature review

This section aims to discuss the available traditional techniques to determine the target cell's RSRP and its limitations. Subsequently, it elucidates the limitations of available data-driven techniques and outlines the advantages of the algorithm proposed in this paper.

Traditionally, Angle of Arrival (AoA) and Angle of Departure (AoD) are preferred to predict CSI¹⁻⁶. However, the next generation communication networks exploits frequencies ranging in sub 6 GHz and THz ranges to promise higher bit rates^{7,8}. Wireless links operating at such frequencies for AVs pose unique challenges where shorter wavelengths and higher frequencies are involved. Among others, high scattering and reflection limit the use of AoAs and AoDs^{9,10}. Therefore, obtaining precise AoA and AoD at these frequencies is challenging and essentially requires measuring target beam and complex calculations^{11,12}.

Correlation-based adaptive compressed sensing (CBACS) exploits poor scattering of higher frequencies to estimate CSI and correlates quantized sensing vectors to determine RSRP¹³⁻¹⁶. However, CBACS is inherently sensitive to channel angle quantization, causing resolution loss¹⁷⁻¹⁹. Therefore, CBACS lacks the preferred correlation margin for signals featuring significant variations and proves suboptimal. Moreover, CBACS significantly depends upon a precise model for signal correlation, therefore even a slight deviation in real correlation structure compared to the anticipated model results in suboptimal performance¹⁴. In scenarios where the correlation prototype is too complex or is tuned to mitigate noise in the data, then CBACS is expected to over-fit results and consequently degrade generalization due to limitations posed by only comparing the received powers of different beams for determining CSI^{14,20}. The authors in^{17,21}, demonstrates that estimating mm-Waves channel by exploiting a large number of antennas and hybrid pre-coding poses a challenge in its own due to limited access to detailed channel dimensions in digital baseband systems, the phenomenon commonly known as channel subspace sampling limitation.

Sparse properties of mm-Waves can be readily exploited for mm-Waves' CSI estimation^{22–26}, also known as Orthogonal Matching Pursuit (OMP). However, OMP shows performance limitations in massive multiple in multiple out (MIMO) applications due to low Signal-to-Noise Ratio (SNR) before beamforming^{17,27}.

Dual connectivity is often employed to obtain target cell bearings by exploiting simultaneous connections with two hosts^{26,28–32}. However, dual connectivity at first is resource intensive, may explode the numbers of unnecessary handover ping-pongs due to simultaneously involving multiple radio circuitries, might challenge the network for co-channel interference, and also unnecessarily utilize channel resources that are already scarce^{17,18,33–35}. Despite limitations of dual connectivity as discussed previously, it is capable of providing accurate CSI as used in^{34,35}.

An advanced technique derived from dual connectivity is multi-connectivity, a technique of choice for most researchers, as suggested in³⁶, where the user is simultaneously connected to multiple hosts, and thus the AV can switch to target cell without an MW. The authors in^{37–40}, suggest using long-short term memory (LSTM) based prediction algorithm to improve HSR. The technique stores previously marked handover points to execute such future decisions. However^{37–40}, used LSTM majorly to improve handover delays and when to handover by previously accumulated data points stored in a database. For the proposed work, we require a technique that can readily be adopted for AVs to work in rapidly changing wireless environments without the requirement of past data points. Therefore, LSTM may underperform in newer test environments where past data is not available. Moreover, LSTM is a blind handover technique as it forces to handover the channel based upon past data points merely, without even evaluating if the wireless channel is actually deteriorated. Also, LSTM algorithm may only function if the wireless channel remains correlated for longer periods, which is rare at ultra-high frequencies such as in mm-Waves and THz.

The authors in^{41–43} use reinforcement learning (RL) for resource management such as energy-efficient traffic offloading from macro to small cells, efficient spectrum sharing in cognitive radios, and robust convergence for independent resource allocation slices. The authors in^{33,44,45} foster the use of RL for CSI determination due to its inherited limitations, such as hit-and-trial-based outputs that effectively increase the time required to converge the objective function and hence increases the model's training period. In⁴⁶, the extensive use of RL is also criticized because overloading the model causes inaccuracy issues. The authors in^{47–49} use kernel-based algorithms to predict positions in wireless sensor environments for sensor localization and CSI estimation.

The authors in⁵⁰ suggest Bayesian regression (BR) making the users to execute a handover before the cell boundary, thus reducing the RSRP gap between the host and target cell. However⁵⁰, does not cover scenarios where the host RSRP may drop due to varying channel behavior while residing inside a cell's boundary. Therefore, BR's effective performance is limited to cell boundaries only.

A dynamic random suppression (RS) mechanism is proposed for improving HSR in⁵¹. The RS algorithm works by developing an elliptic function between vehicle speed and hysteresis, suppressing reverse handovers by introducing normally distributed random variate, thus maintaining high HSR and reduced handover ping-pongs. The RS technique improves HSR by dynamically adjusting the RSRP thresholds since it mainly suppresses reverse handovers and increases handover probability. The authors in^{52,53} propose Q-learning for improving carrier selection by improving time-to-trigger mechanism but do not discuss CSI estimation³³. Q-learning also requires RL schemes that are resource intensive^{33,44,54}, hence is not recommended for the proposed algorithm.

The traditional methodologies discussed above significantly rely on MWs for physically scanning target cell bearings and lack predictive capabilities. In contrast, this study proposes an approach that suppresses the upcoming handover requests if their failure can be determined beforehand. Consequently, such an intelligent system may save a network from unnecessary wireless channel interruptions due to frequent MWs, specifically for handover requests that are already expected to fail. This work advocates for the necessity of a data-driven predictive handover technique in comparison to traditional event-driven handovers for AVs. If such unnecessary MWs are eliminated, the AVs can enjoy improved HSRs together with seamless connectivity.

The proposed work addresses the research limitations of the studies available so far in literature. In particular, we propose a predictive approach to obtain the target cell's CSI in advance, in contrast to scanning target cell's radio bearings while remaining in its serving band. All the classical techniques such as AoA/AoD, CBACS, OMP, dual connectivity and multi-connectivity require live monitoring of target cell's bearings, which is to be avoided according to the proposed approach. Moreover, this work strongly opposes the use of multi-connectivity for the proposed model because, with the increased number of vehicles, the number of simultaneous connections will overload the system due to a higher number of unnecessary handovers and their consequent control signaling. Furthermore, the kernel based algorithm is a popular technique amongst researchers, however, in⁴⁷ the authors restrict the user to traveling in a straight line only in certain scenarios, causing channel modeling limitations, as modern AVs are not restricted to traveling in a straight line. The proposed work assumes that all AVs could freely move within the coverage of cells. The authors in⁵⁰, discuss a boundary limited handover technique (BR) that executes a forceful handover just before a cellular boundary is reached even if the RSRP does not go below threshold. In contrast, the proposed algorithm is not boundary dependent but remains active for all cases where RSRP gets lowered than the set thresholds, predicting real-time RSRP that is not limited to cellular boundaries, and thus can preempt any handover request that is likely to fail.

The technical contributions of this work can be summarized as follows:

1. Development of a path loss model for CSI calculation: this helps the proposed model to calculate RSRP where previous data is unable and provides a solution for predicting mm-Waves CSI while remaining in sub 6 GHz band.
2. Development of an ML model: this provides a statistical solution that identifies the proposed model with training data and then can be used to make predictive decisions regarding success or failure upcoming hand-over request.

3. Generalizing objective function: this helps the proposed model to avoid overfitting because the path loss model can virtually generate RSRP estimates at all the co-ordinates within the coverage area of target base station.
4. Validate prediction estimates: Since the proposed model uses ML and predictive estimates, thus this work exploits receiver operating characteristics area under the curve (ROC-AUC) to validate model's efficiency in predicting true estimates.
5. Dynamic model training period: the proposed model uses two unique training periods depending upon the channel coherence time. This helps the proposed model to collect training samples while the channel is highly correlated.
6. Simulation results: the proposed model operation is shown together with tabulated and graphical results. Furthermore, the improvement in comparison to the baseline algorithm are also discussed.

This work progresses in the following order: Sect. "Path loss model" discusses path loss models that helps in calculating RSRP at a targeted user co-ordinate. Section "Model design" highlights the proposed ML scheme (XGBoost) where the gathered data is used to generate a predictive model. This section also encompasses the algorithm for generating ROC-AUC curves while considering the estimates true if $ROC-AUC \geq 0.7$. Sect. "Sample collection" underscores the importance of sample collection within channel coherence time to precisely model the channel for CSI estimation. Section "Operating principles of the proposed model" discusses the operating model of the proposed design. Section "Simulation results" describes the simulation results whereas Sect. "Conclusion" concludes the work.

Path loss model

In order to materialize the proposed work, the first step is to calculate the path loss model which is detailed in this section. The proposed approach uses the path loss model to calculate expected RSRP for given frequency at a particular co-ordinate within the coverage area. The same path loss models are also used to obtain RSRP training data sets of the proposed model. This work uses two arbitrarily chosen frequency pairs, i.e., 35 GHz (mm-Waves) and 2500 MHz (Sub 6 GHz). It uses Alpha Beta Gamma (ABG) model and Cost-231 model for mm-Waves and sub 6 GHz, respectively, as given by (1) and (2) below. In principle, any other frequency compatible models can also be used by future research²⁷. The path loss according to the ABG model is

$$PL^{ABG} = \alpha + 10\beta \log_{10}(d) + 10\xi \log_{10} \frac{f_c}{1GHz} + \varphi_{\delta}^{ABG} \tag{1}$$

where α and ξ are path loss dependence co-efficient, β is optimized offset parameter, d is the distance between transmitter and receiver, f_c represents carrier frequency and φ_{δ}^{ABG} is a Gaussian random variable showing large scale fluctuations of the signal. The Cost 231 model is expressed as

$$PL^{Cost231} = (46.3 + 33.9 \times \log_{10}(f_c) + 13.82 \times \log_{10} h_{te} - \alpha(h_{re}) + (44.9 - 6.55 \times \log_{10}(h_{te})) \times \log_{10}(d) + C), \tag{2}$$

where f_c is the carrier frequency, h_{te} represents antenna height, $\alpha(h_{re})$ is the frequency correction factor, d denotes the separation distance, and $C = 3$ dB.

The correction factor $\alpha(h_{re})$, is given as

$$\alpha(h_{re}) = 3.2 \times \log_{10}(11.75 \times h_{re})^2 - 4.97 \tag{3}$$

where h_{re} is the receiver height.

Model design

Having the path loss model, the next step is to formulate the model design. The proposed model is based upon a binary prediction classifier to determine whether the estimations are valid or not. Moreover, this work uses supervised learning (SL) and iterative ensemble boosting to convert weak learners into stronger models (both discussed later in this section). The Fig. 2 shows how the proposed model progresses stepwise.

For simulation purposes, this study distributes vehicles in a cell of radius r , with an intensity to show expected vehicles in a given area. Let the total number of vehicles in an area be denoted by N and the coverage area be denoted by A . The vehicles are plotted in r such that $P(f)$ is a stochastic function with a process rate λ and a

probability of M in time f . Let \mathbb{B} define the output of an arbitrary function such that $\lim_{j \rightarrow 0} \left(\frac{\mathbb{B}(j)}{j} = 0 \right)$. Then,

for the proposed algorithm, the vehicles are plotted as per algorithm given by Eqs. (4a-4o)⁵⁵, justifying that the number of occurrences in given time is Poisson-distributed with mean λf , for all $j, t \geq 0$. We have

$$m_0 = (f + j) = M[P(f + g) = 0] \tag{4a}$$

Where,

$$M[P(f) - P(0) = 0, P(f + k) - P(f) = 0] \tag{4b}$$

The independent increments are given as,

$$[IndependentIncrements] = M[P(f) - P(0) = 0] \cdot Q[P(f + j) - M(f) = 0] \tag{4c}$$

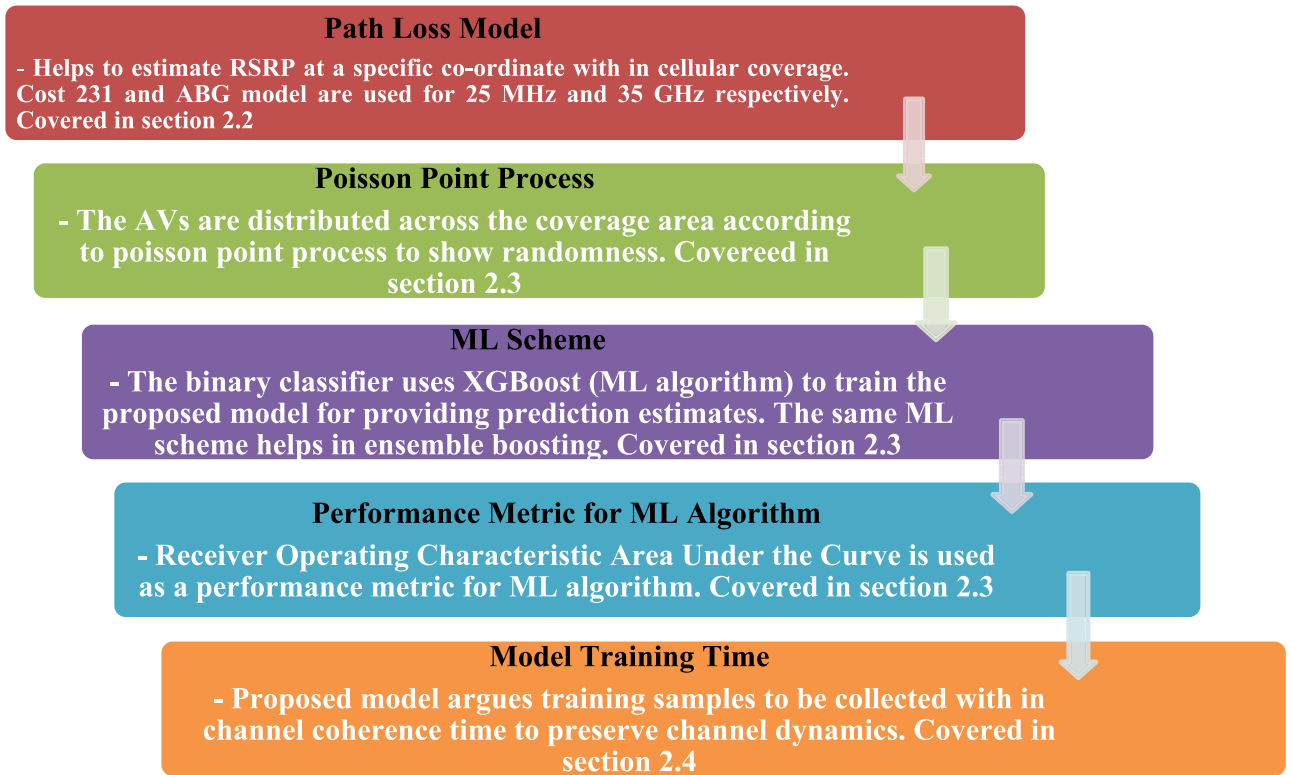


Fig. 2. Proposed model: stepwise details.

And for stationary mobile users,

$$[ForStationary] = M [P(f) = 0] .Q [P(g) = 0] = m_0(f)(1 - \lambda g + c(i)) \tag{4d}$$

therefore

$$\frac{m_0(f+g) - m_0(v)}{g} = -m_0(f)\lambda + \frac{c(g)}{g} \tag{4e}$$

And For

$$g \rightarrow 0^+ \frac{d(m_0(f))}{d(m)} = -m_0(f)\lambda \tag{4f}$$

then,

$$\frac{d(f_0(f))}{d(f_0)} = -\lambda df \tag{4g}$$

when,

$$P > 0, \tag{4h}$$

then,

$$m_n(f+g) = M[P(f+g) = 0] \tag{4i}$$

$$M [P(f) = t, P(f+g) - P(f) = 0] + M [P(f) = P-1, P(f+g) - P(f) = 1] + M [P(f+g) = P, P(f+g) - P(f) \geq 2] \tag{4j}$$

$$= M [P(f) = t] .MP(g) = 0 + MP(f) = P-1.MS(g) = 1 + c(g) \tag{4k}$$

By simplifying (4 k),

$$= (1 - \lambda g) m_s(v) + \lambda g m_{q-1}(v) + c(g) \tag{4l}$$

Since

$$\frac{m_p(f + g) - m_p(f)}{g} = -\lambda m_p(f) + \lambda f_{p-1}(f) + \frac{c(g)}{g} \tag{4m}$$

For

$$g \rightarrow 0^+ \tag{4n}$$

$$\frac{dm_p(f)}{d(f)} = -\lambda m_p(f) + \lambda f_{p-1}(f) \tag{4o}$$

The Fig. 3 provides the flowchart for distributing AVs (resampling from Poisson Point Process) across the coverage area of cell.

The proposed algorithm uses Eqs. (5a-5s) for ensembles' boosting in this work, Input: Training Data $\{(w_i, x_i)\}_{i=1}^N$,

$$\text{Loss function} = K(x, F(w)) \text{ number of weak learners} = L, \text{ Learning rate} = \alpha \tag{5a}$$

initializing models,

$$f_{(0)}(w) = \arg_{\theta} \min \sum_{i=1}^N K(x_i, \theta) \tag{5b}$$

For

$$l = 1 \text{ to } L, \tag{5c}$$

computing gradients,

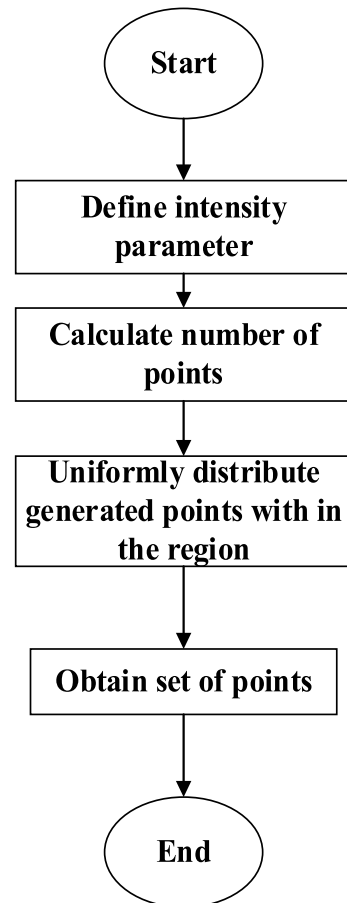


Fig. 3. Flowchart for distributing AVs across the cellular coverage.

$$\hat{g}_l(w_i) = \left[\frac{\partial K(x_i, f(w_i))}{\partial f(w_i)} \right]_{f(w)=\hat{f}_{(l-1)}(w)} \quad (5d)$$

computing Hessians,

$$\hat{h}_l(w_i) = \left[\frac{\partial K(x_i, f(w_i))}{\partial f(w_i)^2} \right]_{f(w)=\hat{f}_{(l-1)}(w)} \quad (5e)$$

using the training set,

$$= \left\{ \frac{\hat{g}_l(w_i) = \left[\frac{\partial K(x_i, f(w_i))}{\partial f(w_i)} \right]_{f(w)=\hat{f}_{(l-1)}(w)}}{\hat{h}_l(w_i) = \left[\frac{\partial K(x_i, f(w_i))}{\partial f(w_i)^2} \right]_{f(w)=\hat{f}_{(l-1)}(w)}} \right\}_{i=1}^N \quad (5f)$$

to fit base learners.

by reducing optimization problem,

$$\hat{\phi}_m = \arg_{\phi} \min \sum_{i=1}^N 0.5 \hat{h}_l(w_i) \left[\phi(w_i) - \frac{\left[\frac{\partial K(x_i, f(w_i))}{\partial f(w_i)} \right]_{f(w)=\hat{f}_{(l-1)}(w)}}{\left[\frac{\partial K(x_i, f(w_i))}{\partial f(w_i)^2} \right]_{f(w)=\hat{f}_{(l-1)}(w)}} \right]^2 \quad (5g)$$

$$\hat{f}_{(l)}(w) = \alpha \hat{\phi}_l(w) \quad (5h)$$

by updating the model,

$$\hat{f}_{(0)}(w) = \hat{f}_{(l-1)}(w) + \hat{f}_l(w) \quad (5i)$$

simplifying the Eq. (5i),

$$\hat{f}(w) = \hat{f}_L(w) = \sum_{l=0}^L \hat{f}_l(w) \quad (5j)$$

for simulation purpose, let the gathered parameters as given in Tables: 1 and 2 (explained later) be denoted by $V(o)$ and individual parameters be given by (O_n) . Then,

$$V(o) = \{V(o)_1, V(o)_2, \dots, V(o)_n\} \quad (5k)$$

for the output W , let E_o be the initial predictive model, then for number of predictive models,

$$w_l \stackrel{E_l}{\leftarrow}, w_l \rightarrow f(E_l) \quad (5l)$$

$E_n \rightarrow (x - E_o)$, associates with residuals.

A new model g_1 generates to fitting the previous step. Therefore, g_1 together with E_o generates E_1 as an improved model. Thus,

$$E_1 = E_0 + g_1 \quad (5m)$$

$$E_2 = E_0 + g_2 \quad (5n)$$

$$E_n = E_0 + g_n \quad (5o)$$

The additive learners technically do not interfere preceding function, however new information improves the previous error. In terms of error, the newer model's error should always be less than the previous model.

Therefore,

$$L_1 < L_0 \quad (5p)$$

$$L_2 < L_1 \quad (5q)$$

$$L_3 < L_2 \quad (5r)$$

$$L_n < L_{n-1} \quad (5s)$$

The proposed algorithm optimizes feature selection by least absolute shrinkage and selector operator (L). The L supports learning model to restrain feature quantity while providing sparse solutions, and helps in optimizing

computational loads by avoiding coefficients with zero features. Moreover, (L) provides solutions for essential time-based regression challenges by adapting variety of variables. The compressional readiness of (L) helps in achieving quick sparse features and provides robust predictions by reducing data points towards their expected mean. The Lagrangian form of (L) is given by Eq. (6), where x_i is the response for i^{th} , $(L)_0$ denotes intercept, g_{ij} is the regressor coefficient and λ defines the scaling factor:

$$(L) = \arg(L) \min \left[0.5 \sum_{i=1}^N \left(x_i - (L)_0 - \sum_{j=1}^p g_{ij}(L)_j \right)^2 + \lambda \sum_{j=1}^p \|(L)_j\| \right] \tag{6}$$

The mean square error (MSE) of the estimator is calculated by squared normalized bias sum and is given by Eq. (7) insert reference,

$$\text{MSE} \left((\tilde{L})_{\lambda} : G \right) = \mathbf{E} \left[\|\tilde{(L)}_{\lambda} - \tilde{(L)}\|^2 : G \right] \tag{7}$$

Equation (8) is the expanded version of Eq. (7),

$$\text{MSE} \left((\tilde{L})_{\lambda} : G \right) = \text{trace} \left(\mathbf{Var} \left((\tilde{L})_{\lambda} : G \right) \right) + \text{bias} \left\| \left((\tilde{L})_{\lambda} : G \right) \right\|^2 \tag{8}$$

Assuming that ordinary least squares (OLS) estimator is initialized to zero, then the MSE is given by Eq. (9),

$$\text{MSE} \left((\tilde{L})_{\lambda} : G \right) = \text{trace} \left(\mathbf{Var} \left((\tilde{L})_{\lambda} : G \right) \right) \tag{9}$$

The difference between two MSEs is given by Eq. (9a),

$$\Delta \text{MSE} = \text{MSE} \left((\tilde{L}) : G \right) - \text{MSE} \left((\tilde{L})_{\lambda} : G \right) \tag{9a}$$

Similarly, the expanded form of Eq. (9a) is given by Eq. (9b),

$$\text{MSE} = \underbrace{\text{trace}(\mathbf{Var}(\tilde{L} : G) - \mathbf{Var}(\tilde{v}_{\lambda} : G))}_{\text{lower ridge variance}} - (\text{minus}) \underbrace{\|\text{bias}(\tilde{v}_{\lambda} : G)\|}_{\text{ridge having higher bias}} \tag{9b}$$

The hyper parameters for the proposed model are given ins Table 1

Since this work uses predictive estimates, therefore model’s performance evaluation is mandatory to determine the validity of the said estimates. For this purpose, this work uses ROC-AUC as a performance metric to validate the predictive estimates. The ROC-AUC is a fundamental metric to evaluate the performance of a binary classifier⁵⁶, this technique helps in issuing an assessment of proposed models ability to discriminate between true versus false positive rate.

The ROC-AUC is plotted as suggested in⁵⁶⁻⁵⁸. Let W and Z denote two random variables respectively, with the distribution functions given by E and H , let e and h be density functions, assuming $E^* = 1 - E$ and $H^* = 1 - H$ denotes survival functions respectively,

The proposed work adopts $W < Z$ stochastically, as per condition given by Eq. (10),

$$E^*(w) \leq H^*(w) \text{ for all values of } w \in (-\infty, +\infty) \tag{10}$$

Similarly,

Feature	Value	Feature	Value
<i>Depth_{max}</i>	6, 8	Complexity control	0, 0.002
Child weights	0, 10	Samples weight	0.5, 0.7
Samples weight	0.5, 0.7	Lambdas	0, 1, 2
Cross validation	5	Estimator number	500

Table 1. Hyper parameters.

Let $\lambda_E(w) = e(w)/E^*(w)$ and $\lambda_G(w) = h(w)/H^*(w)$ represents decay rate of W and Z respectively. Then $W < Z$, if $\lambda_E(w) \geq \lambda_H(w)$ for $w \geq 0$.

Now considering,

$\varphi_E(w) = e(w)/E(w)$ and $\varphi_H(w) = h(w)/H(w)$, the reversed decay rate functions of W and Z respectively are expected to be $W \leq Z$. Therefore $e(w)/E(w) \leq h(w)/H(w)$ as given by Eq. (11),

$$\varphi_E(w) \leq \varphi_H(w) \text{ for } w \geq 0 \quad (11)$$

Or equivalently,

W_t and Z_t denotes random variables at time t , then the reversed decay function at t is given by Eqs. (12 and 13),

$$W_t = W - t; W > t \quad (12)$$

And

$$Z(t) = Z - t; Z > t \quad (13)$$

Stochastically, it is expected that likelihood of $W < Z$.

The Fig. 4 provides the flowchart for implementing the ML scheme (XGBoost) for the proposed model as discussed in Sect. “Model design”

Sample collection

The proposed model uses ML to predict RSRP of the target cell. Therefore, to train the proposed model, the ML scheme requires training data. In particular, the training data is used to model the channel of the target cell. The training samples collected within the channel coherence time (T_C) naturally enhance the true depiction of the target channel.

Generally, in ML schemes, 70% of total data is used for training, and the remaining 30% is used for testing data^{59–62}. If T_C is involved then 70–30% data split generates inaccuracies since samples breaching T_C limits are involved in training the model¹⁸. Therefore, the proposed work suggests that for accurate channel modeling and preserving channel dynamics, samples collected within T_C limits should train the model (modeling highly correlated channel)³³. Since T_C statistically measures the duration over which channel impulse response is invariant, it is proposed that 70% of total samples for model training must only be used if those samples lie within T_C limits.

T_C over which the channel remains coherent is given by⁶³

$$T_C = \frac{3 \times 10^8}{f_{CUE} \sin \varnothing} \quad (14)$$

where f_C refers to the carrier frequency, v_{UE} is the vehicle’s speed and \varnothing is the angle between direction of BS and the vehicle. However, this work does not use (14) to estimate T_C , since the mm-Waves’ antennas are high beam forming and compensate for isotropic path loss. Therefore, the beam forming increases T_C in directional arrays while focusing the signal power on beamwidth-defined angular space toward a user³³. (14) also demands \varnothing but due to high scattering and reflection involved at higher frequencies (such as in mm-Waves and beyond), calculating a single source \varnothing for non-line-of-sight (NLoS) applications becomes complicated, and requires complex radio circuitry. Thus, (14) restricts the model to Line of Sight (LoS) applications only, whereas this research intends to propose a model whose performance is not limited to LoS applications.

T_C can also be calculated as^{63,64}

$$T_C = \frac{D\vartheta}{0.5v_{UE} \sin \varnothing} \quad (15)$$

where D refers to Euclidean distance between the source and the receiver and ϑ refers to the beamwidth. Again, calculating T_C using (15) requires complex radio circuitry to lock on accurate timing advance for estimating the vehicle’s position. Moreover, (15) also demands \varnothing for T_C calculation, whose limitations have already been discussed above. This work assumes vehicles to be stochastically distributed over randomly varying T_C . Therefore, calculating an accurate frame length for cell concentric T_C becomes mathematically complex. This conservative notion is also supported by the fact that the serving station may not be aware of vehicles’ parameters such as distance and serving beam angle. Thus, to add generality, the proposed work another equation to estimate T_C ^{65–67}

$$T_C = \frac{1}{f_m}, f_m (\text{maximum dopplershift}) = \frac{V_{UE}}{\lambda} \quad (16)$$

However, with the advancements in the radio circuitry, researchers can use even more accurate T_C models in the future. For scenarios where 70% of training samples lie within the T_C limits, the training period (T_p) for proposed model is given as

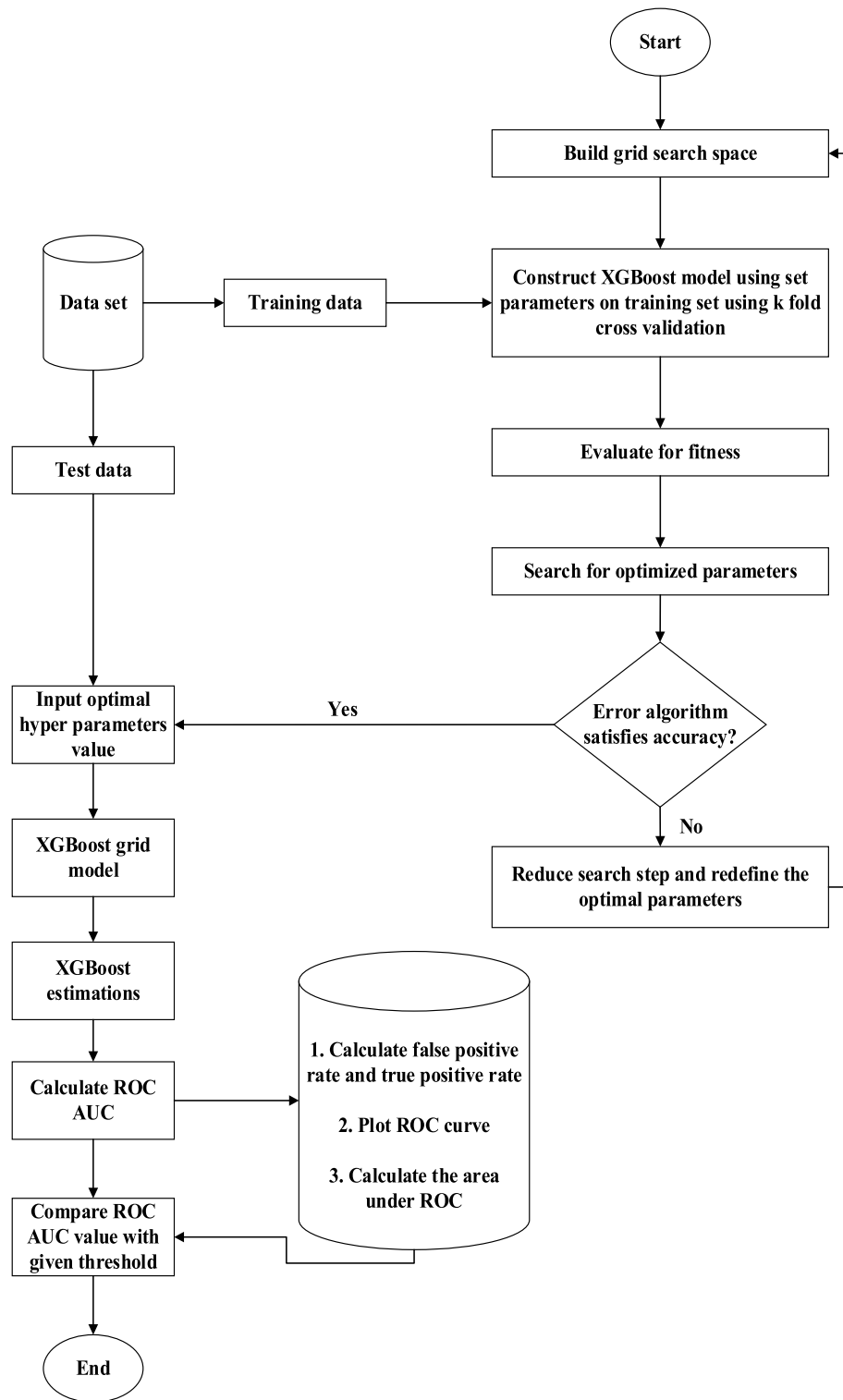


Fig. 4. Flow chart for implementing ML scheme (XGBoost).

$$T_p = 0.7 \times T_s, \text{ for cases where } (0.7 \times T_s) \leq T_C; T_s = \text{simulationtime} \quad (17)$$

Overall, T_p for proposed model is obtained using the following formulas

$$T_p = T_C = \frac{V_{UE}}{\lambda}, \text{ for cases where } (0.7 \times T_{sim}) > T_C \quad (18)$$

$$T_p = T_C = (0.7 \times T_{sim}), \text{ for cases where } (0.7 \times T_{sim}) \leq T_C \quad (19)$$

By using (18) and (19), the proposed model training time never breaches T_C limits and guarantees model learning with samples collected from a highly coherent channel only. Further details regarding performance degradation caused by breaching T_C limits are given in⁶⁸.

As the complete design of the proposed model is discussed above, Table 2 provides details regarding the radio parameters such as path loss model arguments, base station parameters, AV density and speed ranges, and simulation timings for the home and target cell for simulation purposes.

Operating principles of the proposed model

The Fig. 5 shows operating principles of the traditional and proposed model. In the following details, the traditional algorithm will be referred to as a baseline algorithm. In the baseline algorithm, the steps such as initiation of MW, scanning of target cell bearings, and preparation of measurement reports are all event-driven. The baseline model lacks any predictive capabilities that could help in estimating the outcome of the handover request. This event-based technique does not guarantee successful execution of handover requests, and keeps on interrupting cellular traffic for unnecessary MWs without any prior knowledge of its outcome, thus seriously interfering with network smooth traffic flow.

On the other hand, in the proposed algorithm, the steps leading to link interruption are now data-driven and use a predictive technique, avoid unnecessary MWs, guarantee handover success for the requests whose estimations are correctly predicted by the proposed model, and ensure robust connection with the host.

Simulation results

This section details the simulation results (HSR improvements) in comparison to the baseline algorithm after incorporating the proposed technique. The Fig. 6 demonstrates working mechanism of the proposed model by showing an arbitrarily chosen AV#177 moving at an average speed of 83 km/hr. The grey area in Fig. 6 shows the learning period where the proposed model follows the baseline algorithm to collect training samples within T_C . Beyond this point, the proposed mechanism allows for the prediction of the success or failure of the upcoming handover request. Therefore, as indicated in Fig. 6, at $T_S = 78$ ms and 88 ms, the proposed mechanism preempts handover requests that are likely to fail, and hence avoids unnecessary MWs. On the other hand, the baseline algorithm, unaware of failing upcoming handovers, opens the MWs for scanning target cell bearings, hence unnecessarily interrupting the communication channel two times and also causing two handover failures. The Table 3 shows that for AV#177 when the learning period is over, there are seven handover requests in total out of which the baseline algorithm executes five handover requests successfully, for remaining two handover requests the MWs are engaged at the cost of interrupting data traffic but are unsuccessful. On the other hand, the proposed algorithm is already aware of these two inbound handover failures in advance. Thus it readily preempts these handover requests and avoids unnecessary MWs to guarantee smooth traffic flow.

According to the simulation results shown in Fig. 6 and Table 3, the HSR for AV#177 is 71.42% using the baseline and 100% for the proposed algorithm respectively. The Fig. 7 shows the changing RSRP levels for both sub 6 GHz frequency and mm-Wave frequency for AV#177 over the simulation period of 100 ms. The Fig. 8 shows the operating characteristics of the receiver with the area under the curve (ROC-AUC) validating the predicted estimates and showing prediction accuracy. The ROC in Fig. 8, shows the performance of proposed binary classifier which in our case is the ML algorithm's performance across the recommended threshold. The AUC under the ROC curve in Fig: 8, demonstrates the prediction efficiency of the proposed ML model. For the simulation purposes the predicted estimates are valid if $\text{ROC-AUC} \geq 0.7$. For the AV#177 the ROC-AUC is equal to 0.996. The Fig. 9 shows AVs' distribution around the base station (BS), in this simulation there are

Parameter	Value	Parameter	Value
Cell radius	350 m	Antenna Height	36 m
$f_1 = 38$ GHz (mm-Waves)	ABG Model	Antenna Gain	$f_1 = 24$ dBi and $f_2 = 17$ dBi
$f_2 = 2500$ MHz (Sub 6 GHz)	Cost 231 Model	Poisson Point Parameter	2×10^3
Base Station Power	46 dBm	Vehicle speed	\ddot{u} 120 km/hr
f_1 bandwidth	100 MHz	Floating intercept values (α, β, φ)	116.77, 0.41, 5.96
f_2 bandwidth	20 MHz	T_{Sim}	100, 200, ..., 0.1000 ms (100 ms offset)

Table 2. Radio parameters.

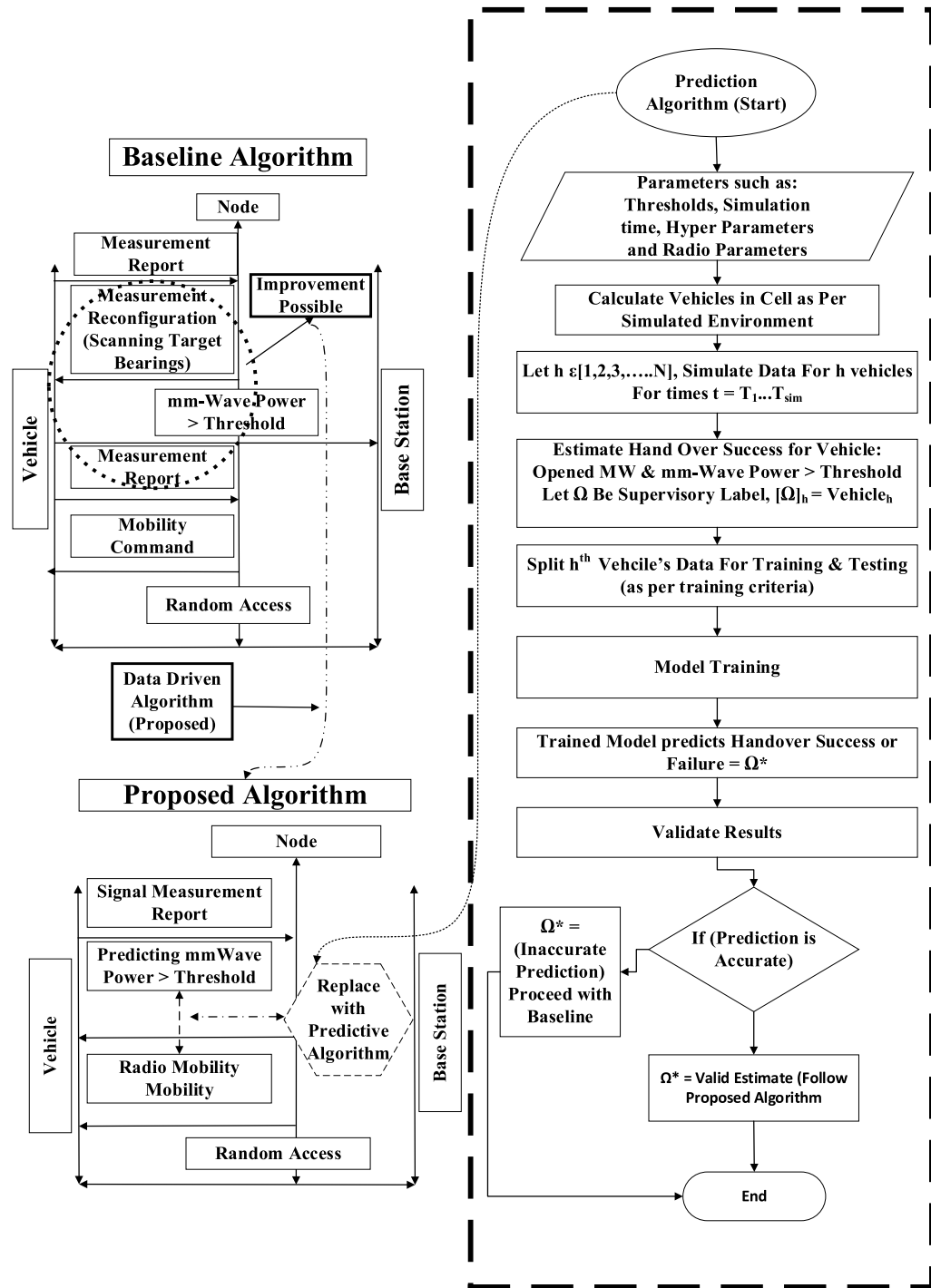


Fig. 5. Baseline vs. proposed model.

774 AVs with in the coverage of base station amongst which the AV#177 is arbitrarily chosen for explaining the concept of proposed mechanism.

The AV#177 is assigned an arbitrary bandwidth of 10Mbits/s. From the Fig. 10 at $T_S = 78$ ms and 88 ms for the proposed algorithm, it can be inferred that the data rate does not drop to 0 Mbits/sec as in the case for baseline algorithm due to active MWs (assuming channel is not degraded by any other external sources). Therefore, the proposed algorithm succeeds in avoiding unnecessary transmission interruptions and guarantees smooth traffic flow. The Fig. 11 shows the instantaneous speed of vehicle AV#177 for the complete simulation run.

The Table 4 shows the results obtained at the network level with an average number of 774 vehicles, with their speed ranging from 0 km/hr to 120 km/hr (refer to¹⁷, for varying densities). The Table 4 indicates that for $100ms \leq T_S \leq 1000ms$ the average HSRs for the baseline and the proposed algorithms are 93.52% and 97.50%, respectively, i.e., the proposed algorithm improves the average HSR by 3.87%. Since the proposed

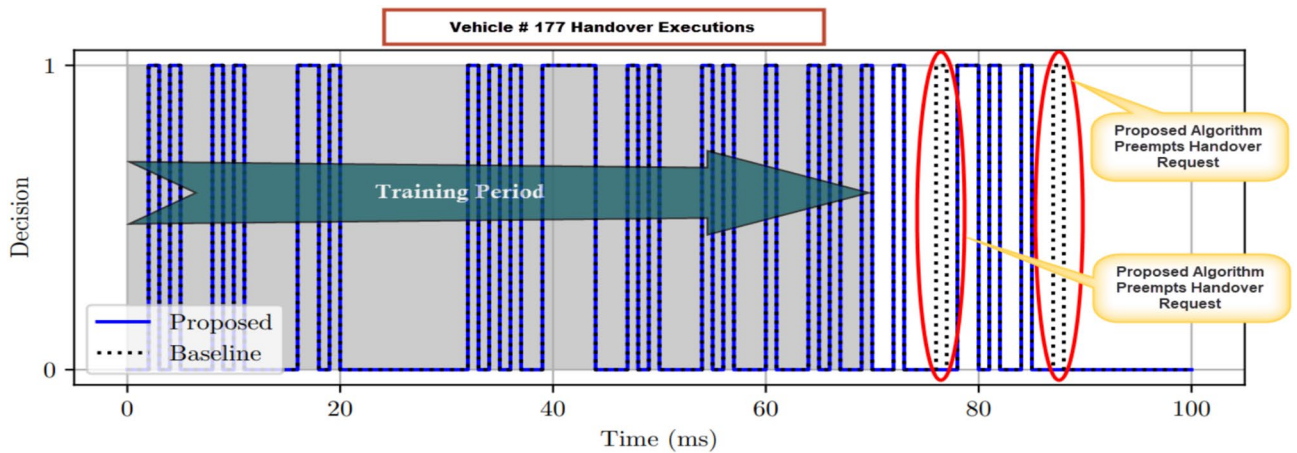


Fig. 6. AV#177 baseline vs. proposed algorithm comparison.

Simulation Time (T_s)	Baseline Algorithm			Proposed Algorithm			
	Total Handover Attempts (Baseline Algorithm)	Handover Failures (Baseline Algorithm)	Baseline Algorithm HSR (%)	Training Period (T_C)	Total Handover Attempts (Baseline Algorithm)	Handover Failures (Baseline Algorithm)	Baseline Algorithm HSR (%)
100	7	2	71.42	70	5	0	100

Table 3. Baseline vs. proposed algorithm HSR comparison for vehicle#177.

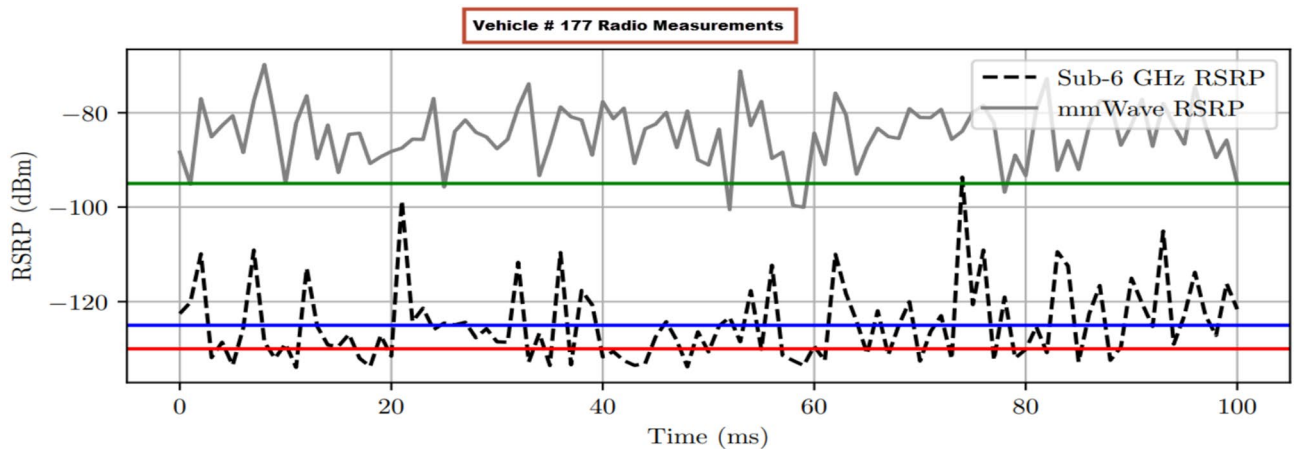


Fig. 7. AV#177 RSRP for sub 6 GHz and mm-Wave band.

algorithm is already aware of the target cell’s radio bearings, it only allows handover requests that are likely to succeed and is pre-empting handover requests that are expected to fail.

The Fig. 12 shows the HSR of the baseline and the proposed algorithm as given in Table 4 with respective simulation times. From Fig. 12 it is clear that the proposed algorithm significantly improves HSR, since for the baseline algorithm the HSR remains within the range of $93.03\% \leq HSR_{traditional} \leq 94.35\%$, whereas for the proposed algorithm HSR remains within the range of $97.40\% \leq HSR_{proposed} \leq 97.67\%$.

The Fig. 13 and 14 (original image split into two for clarity) show the number of bits transferred per each T_s with the baseline and the proposed algorithm, respectively. As it can be observed, due to no advance information regarding upcoming handover request failures, the baseline algorithm unnecessarily opens MWs for scanning target cell bearings at the expense of data transmission interruption, thus degrading data transmission rates at their respective periods. Therefore, the number of bits transferred by the baseline algorithm for each T_s is significantly lower compared to the proposed algorithm. In contrast, with the proposed algorithm, the bits transfer rate remains consistent due to circumventing frequent data traffic interruptions by avoiding unnecessary MWs. Therefore, Figs. 13 and 14 show higher number of bits transferred at each T_s for the proposed algorithm

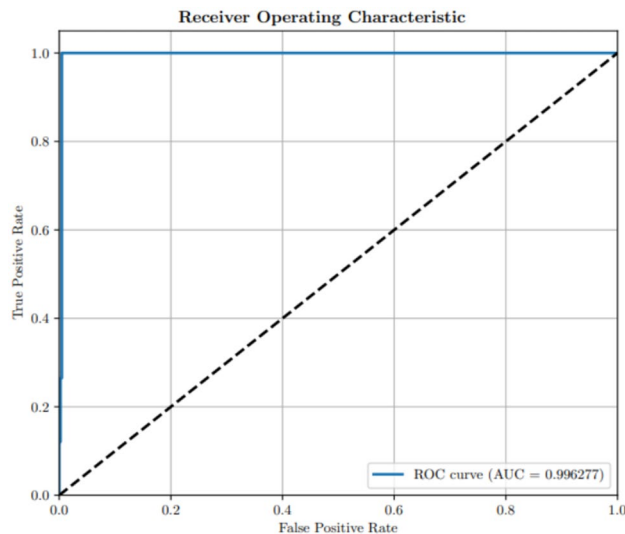


Fig. 8. ROC Curve (AUC > 0.7).

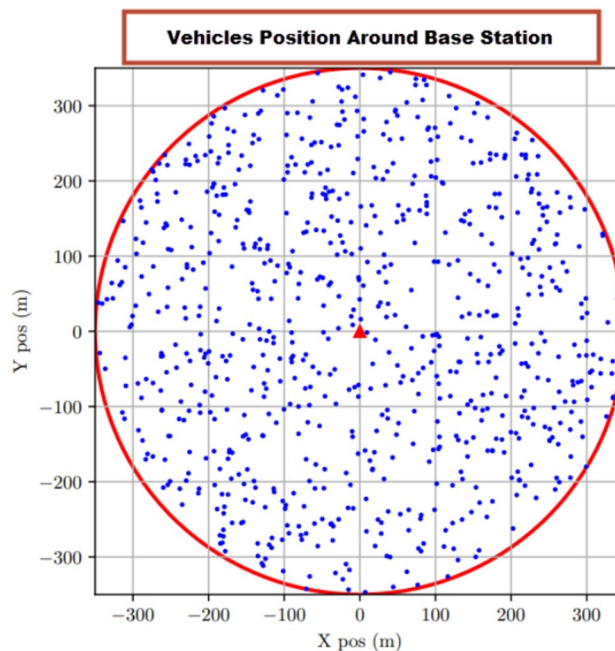


Fig. 9. AVs position relative to base station (Total AVs = 774).

respectively. The Fig. 15 shows a difference between the proposed and baseline algorithm total bits transfer per simulation period for each T_s .

The Fig. 16 shows the error bar charts for the baseline and the proposed algorithm, where the mean $HSR_{baseline} = 93.75\%$ with standard deviation (δ) = 0.43 and $HSR_{proposed} = 97.49\%$ with $\delta = 0.07$, respectively. The standard deviation is lower for the proposed algorithm since the data driven model determines the outcome of the upcoming handover request in advance, thus preempts the handover requests that are likely to fail, making the HSR smoother and improved for each simulation run.

This work also conducts TTest to ensure the significance of results. For simulation results (HSR), the significance value (p) is $3.024E - 10$ which determines that our results are significant and the proposed algorithm is an effective tool for improving HSR. The Table 5 summarizes the complete obtained simulation results as discussed throughout the Sect. “Simulation results”.

Although the simulation results are impressive still the proposed work lacks real world testing. However, other authors investigating similar domain also used simulation based results to justify their proposed schemes

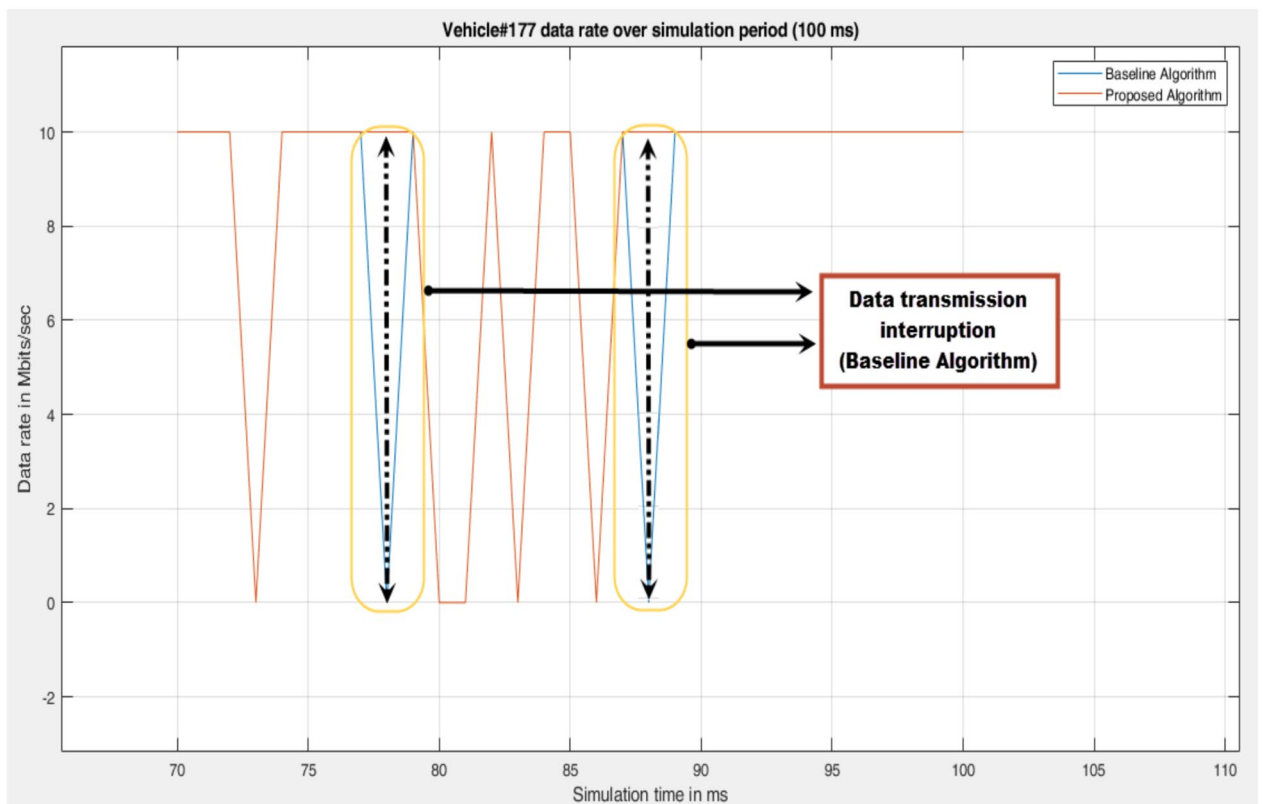


Fig. 10. AV#177 proposed algorithm avoids data rate interruption.

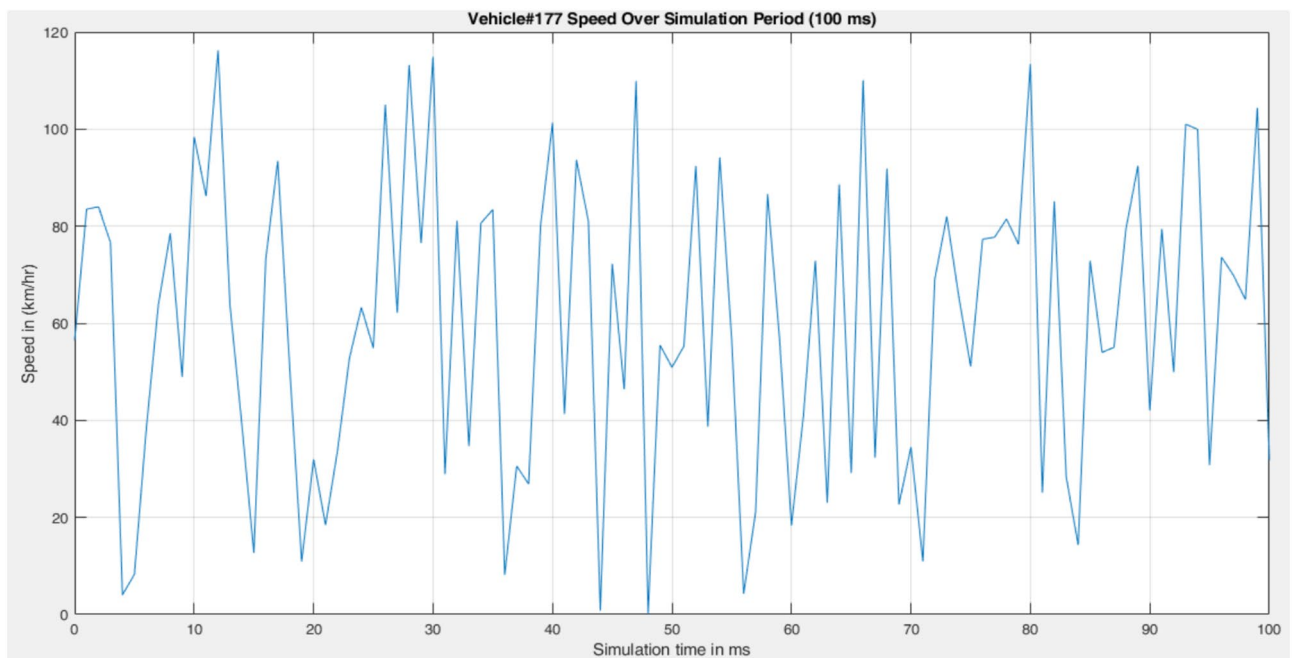


Fig. 11. Vehicle#177 speed curve.

Simulation Time (T_S) ms	Training Period (T_P) ms	Handover Attempts	Baseline Algorithm Successful Attempts	Proposed Algorithm Successful Attempts	Baseline Algorithm Failure	Proposed Algorithm Failure	Baseline HSR (%)	Proposed HSR (%)	Δ HSR (%)
1000	295	223,229	9482	9789	568	261	94.35	97.40	3.05
900	328	181,234	18,241	19,026	1287	502	93.40	97.43	4.03
800	328	181,234	26,949	28,291	2016	674	93.04	97.67	4.63
700	421	88,715	36,247	37,600	2303	950	94.03	97.54	3.51
600	420	57,422	44,989	46,674	2900	1215	93.94	97.46	3.52
500	350	47,889	54,179	55,982	3243	1440	94.35	97.49	3.14
400	280	38,550	83,161	86,474	5554	2241	93.74	97.47	3.73
300	210	28,965	168,948	176,696	12,286	4538	93.22	97.50	4.28
200	140	19,528	169,948	176,696	11,286	4538	93.77	97.50	3.72
100	70	10,050	209,229	217,704	14,000	5525	93.73	97.52	3.80

Table 4. Network level results for baseline vs. proposed algorithm.

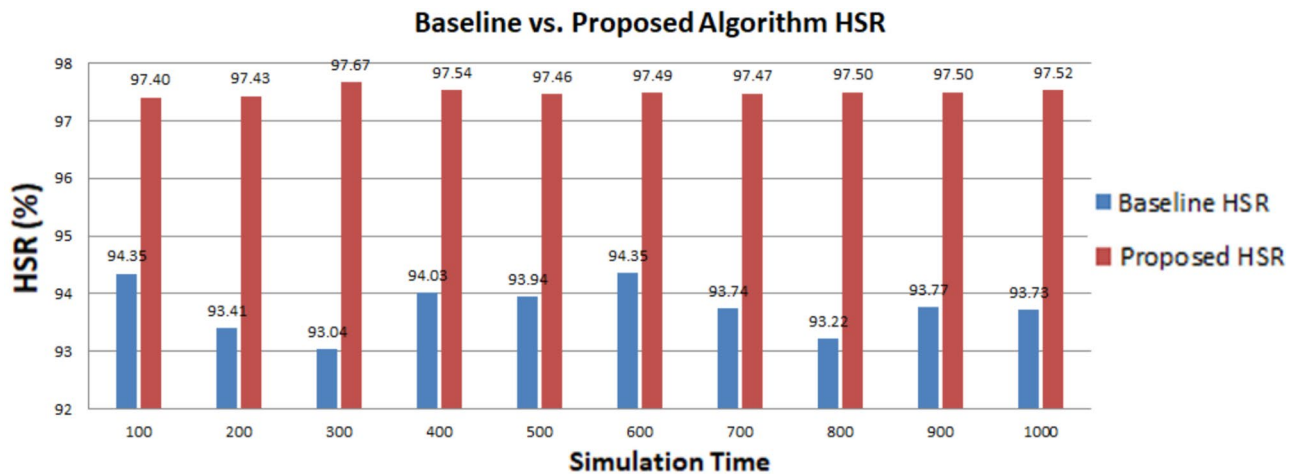


Fig. 12. Baseline vs. proposed HSR.

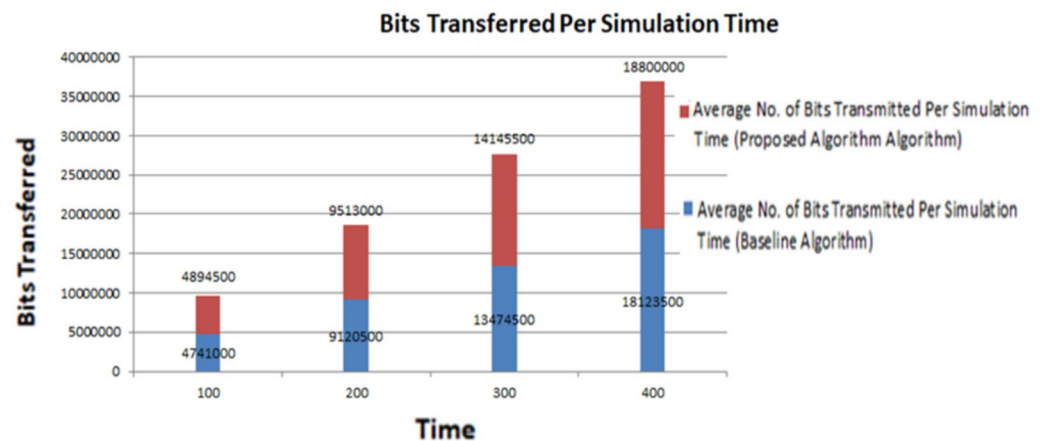


Fig. 13. Bits transfer per simulation time up to 400 ms.

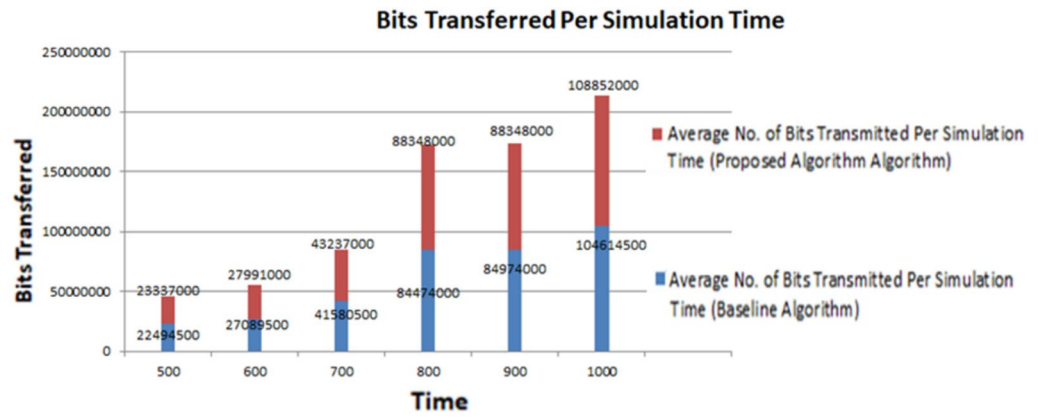


Fig. 14. Bits transfer per simulation time for 500 ms and higher.

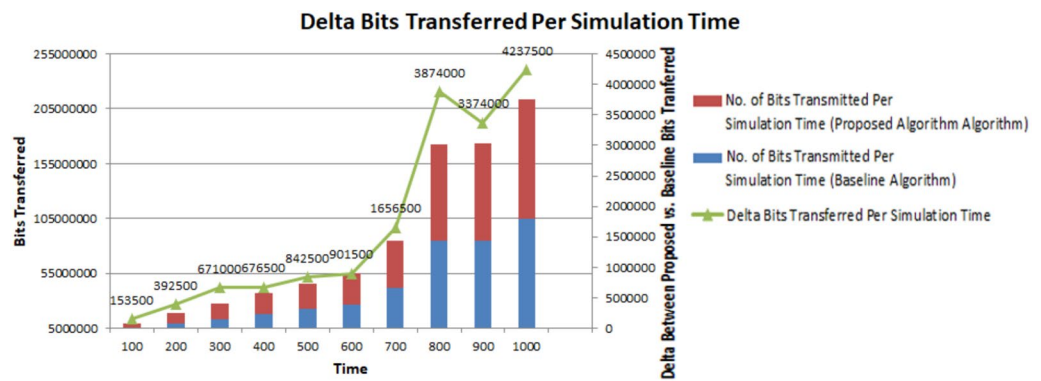


Fig. 15. Difference between transmitted bits for baseline vs. proposed algorithm.

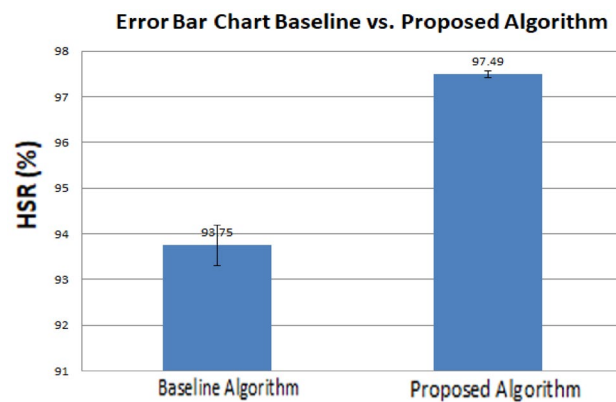


Fig. 16. Error bar chart.

Parameter	Value
Average $HSR_{baseline}$	93.75%
Average $HSR_{proposed}$	97.49%
Std. Dev $HSR_{baseline}$	0.43
Std. Dev $HSR_{proposed}$	0.07
TTest (p)	3.024E-10

Table 5. Results summary.

such as in^{69–71} because simulator based results in its self are quite a challenge to perform and are always used before real world testing.

Conclusion

To provide an integrated solution to the challenge of seamless mobility, this paper has demonstrated and compared the effectiveness of data-driven enhanced extreme gradient boosting technique in predicting target cell's RSRP compared to the traditional event-driven approach. From the test results, it is clear that by using ML, advance information regarding the success or failure of an upcoming handover can be readily estimated, and hence a network can effectively avoid unnecessary MWs. This methodology has effectively eliminated the conventional real-time target cell's bearer measurements where an AV sacrifices the communication channel and suspends data traffic to trigger an MW. The proposed technique has improved the HSR by keeping sessions in the most optimum band and has avoided unnecessary handover requests. The simulation results suggest that for the proposed algorithm the achieved HSR was 97% compared to baseline algorithm which was 93%. This tremendous enhancement in results shows the effectiveness of the proposed algorithm for the mobility management of autonomous vehicles from sub 6 GHz to mm-Waves networks.

In future, ML will be considered for improving the signal quality and hybrid beam forming together with RSRP prediction. Field-testing for confirming the feasibility of the proposed solution in actual AV deployments will authenticate the simulated results.

Data availability

"The datasets used and/or analysed during the current study available from the corresponding author on reasonable request."

Received: 8 February 2025; Accepted: 26 May 2025

Published online: 01 July 2025

References

- Zhu, D., Choi, J. & Heath, R. W. Auxiliary beam pair enabled AoD and AoA estimation in closed-loop large-scale millimeter-wave MIMO systems. *IEEE Trans. Wireless Commun.* **16**(7), 4770–4785 (2017).
- Dutty HB, Mowla MM. Channel modeling at unlicensed millimeter wave V band for 5G backhaul networks. In 2019 5th International Conference on Advances in Electrical Engineering (ICAEE) Sep 26 (pp. 769–773). IEEE. (2019).
- Song, X., Haghghatshoar, S. & Caire, G. Efficient beam alignment for millimeter wave single-carrier systems with hybrid MIMO transceivers. *IEEE Trans. Wireless Commun.* **18**(3), 1518–1533 (2019).
- Dahal S, Stephanou EA, Talukdar N, Ahmed S, King H, Faulkner M. Millimetre wave propagation reverse measurements for 5G urban micro scenario. In 2019 IEEE 89th Vehicular Technology Conference (VTC2019-Spring) Apr 28 (pp. 1–5). IEEE. (2019).
- Garcia, N., Wymeersch, H. & Slock, D. T. Optimal precoders for tracking the AoD and AoA of a mmWave path. *IEEE Trans. Signal Proc.* **66**(21), 5718–5729 (2018).
- Qin, Q., Gui, L., Cheng, P. & Gong, B. Time-varying channel estimation for millimeter wave multiuser MIMO systems. *IEEE Trans. Veh. Technol.* **67**(10), 9435–9448 (2018).
- Miao H, Zhang J, Tang P, Tian L, Zhao X, Guo B, Liu G. Sub-6 GHz to mmWave for 5G-advanced and beyond: Channel measurements, characteristics and impact on system performance. *IEEE Journal on Selected Areas in Communications*. May 8. (2023).
- Halamandaris A, Alam MS, Ahmed I, Hasan K, Kaddoum G. Performance analysis of 6G communication links in the presence of phase noise. In 2023 IEEE Latin-American Conference on Communications (LATINCOM) Nov 15 (pp. 1–6). IEEE. (2023).
- Martínez-Inglés, M. T., Rodríguez, J. V., Pascual-García, J., Molina-García-Pardo, J. M. & Juan-Llácer, L. On the influence of diffuse scattering on multiple-plateau diffraction analysis at mm-Wave frequencies. *IEEE Trans. Antennas Propag.* **67**(4), 2130–2135 (2019).
- Ma J, Shrestha R, Zhang W, Moeller L, Mittleman DM. Scattering Analysis of Terahertz Wireless Links by Rough Surfaces. In 2019 44th International Conference on Infrared, Millimeter, and Terahertz Waves (IRMMW-THz) Sep 1 (pp. 1–2). IEEE. (2019).
- Lee H, Kim S, Choi J. Efficient channel AoD/AoA estimation using widebeams for millimeter wave MIMO systems. In 2019 IEEE 20th International Workshop on Signal Processing Advances in Wireless Communications (SPAWC) Jul 2 (pp. 1–5). IEEE. (2019).
- Zhang, W., Dong, M. & Kim, T. MMV-based sequential AoA and AoD estimation for millimeter wave MIMO channels. *IEEE Trans. Commun.* **70**(6), 4063–4077 (2022).
- Yang H, Fan Y, Liu D, Zheng Z, Lin S. Compressive sensing and prior support based adaptive channel estimation in massive MIMO. In 2016 2nd IEEE International Conference on Computer and Communications (ICCC) Oct 14 (pp. 1618–1622). IEEE. (2016).
- Yang J, Wei Z, Zhang X, Li N, Sang L. Correlation based adaptive compressed sensing for millimeter wave channel estimation. In 2017 IEEE Wireless Communications and Networking Conference (WCNC) Mar 19 (pp. 1–6). IEEE. (2017).
- Rusu C, González-Prelcic N, Heath RW. Low resolution adaptive compressed sensing for mmWave MIMO receivers. In 2015 49th Asilomar Conference on Signals, Systems and Computers Nov 8 (pp. 1138–1143). IEEE. (2015).
- Sun S, Rappaport TS. Millimeter wave MIMO channel estimation based on adaptive compressed sensing. In 2017 IEEE international conference on communications workshops (ICC Workshops) May 21 (pp. 47–53). IEEE. (2017).
- Majid, S. I., Shah, S. W. & Marwat, S. N. Applications of extreme gradient boosting for intelligent handovers from 4g to 5g (mm waves) technology with partial radio contact. *Electronics* **9**(4), 545 (2020).
- Majid, S. I. et al. Using an efficient technique based on dynamic learning period for improving delay in AI-based handover. *Mob. Inf. Syst.* **2021**, 1–9 (2021).
- Hu, C., Dai, L., Mir, T., Gao, Z. & Fang, J. Super-resolution channel estimation for mmWave massive MIMO with hybrid precoding. *IEEE Trans. Veh. Technol.* **67**(9), 8954–8958 (2018).
- Alkhateeb, A., El Ayach, O., Leus, G. & Heath, R. W. Channel estimation and hybrid precoding for millimeter wave cellular systems. *IEEE J. Select. Topics Sign. Proc.* **8**(5), 831–846 (2014).
- Zhou, Z. et al. Low-rank tensor decomposition-aided channel estimation for millimeter wave MIMO-OFDM systems. *IEEE J. Sel. Areas Commun.* **35**(7), 1524–1538 (2017).
- Yeh CC, Hsu KN, Chi JC, Huang YH. Adaptive simultaneous orthogonal matching pursuit for mmWave hybrid beam tracking. In 2018 IEEE 23rd International Conference on Digital Signal Processing (DSP) Nov 19 (pp. 1–5). IEEE. (2018).
- Lee, J., Gil, G. T. & Lee, Y. H. Channel estimation via orthogonal matching pursuit for hybrid MIMO systems in millimeter wave communications. *IEEE Trans. Commun.* **64**(6), 2370–2386 (2016).

24. Zhong, W., Xu, L., Zhu, Q., Chen, X. & Zhou, J. MmWave beamforming for UAV communications with unstable beam pointing. *China Commun.* **16**(1), 37–46 (2019).
25. Weiland L, Stöckle C, Würth M, Weinberger T, Utschick W. OMP with grid-less refinement steps for compressive mmWave MIMO channel estimation. In 2018 IEEE 10th Sensor Array and Multichannel Signal Processing Workshop (SAM) Jul 8 (pp. 543–547). IEEE. (2018).
26. Uwaechia AN, Mahyuddin NM, Ain MF, Latiff NM, Za'bah NF. On the spectral-efficiency of low-complexity and resolution hybrid precoding and combining transceivers for mmWave MIMO systems. *IEEE Access.* Aug 7;7:109259–77. (2019).
27. Mismar FB, Evans BL. Partially blind handovers for mmWave new radio aided by sub-6 GHz LTE signaling. In 2018 IEEE International Conference on Communications Workshops (ICC Workshops) May 20 (pp. 1–5). IEEE. (2018).
28. Monteiro VF, Sousa DA, Maciel TF, Cavalcanti FR, e Silva CF, Rodrigues EB. Distributed RRM for 5G multi-RAT multiconnectivity networks. *IEEE Systems Journal.* Jun 11;13(1):192–203. (2018).
29. Ying G, Qingmin M, Xiaoming W. Energy-optimized 5G dual connectivity radio resource allocation. In 2019 IEEE 2nd International Conference on Electronics Technology (ICET) May 10 (pp. 126–130). IEEE. (2019).
30. Polese, M., Giordani, M., Mezzavilla, M., Rangan, S. & Zorzi, M. Improved handover through dual connectivity in 5G mmWave mobile networks. *IEEE J. Sel. Areas Commun.* **35**(9), 2069–2084 (2017).
31. Ghosh, A. et al. Millimeter-wave enhanced local area systems: A high-data-rate approach for future wireless networks. *IEEE J. Sel. Areas Commun.* **32**(6), 1152–1163 (2014).
32. Chen, J., Wang, Y., Li, Y. & Wang, E. QoE-aware intelligent vertical handoff scheme over heterogeneous wireless access networks. *IEEE Access.* **9**(6), 38285–38293 (2018).
33. Majid, S. I. et al. Optimizing cell selection for data services in mm-waves spectrum through enhanced extreme gradient boosting. *Results Eng.* **6**, 101868 (2024).
34. Nguyen MT, Song J, Kwon S, Kim S. Power allocation for adaptive-connectivity wireless networks under imperfect CSI. *IEEE Transactions on Communications.* May 17. (2023).
35. Kim JS, Park SG, Choi YS. Multi Carrier Cell management and mobility enhancement. In 2023 14th International Conference on Information and Communication Technology Convergence (ICTC) Oct 11 (pp. 1149–1151). IEEE. (2023).
36. Zhao F, Tian H, Nie G, Wu H. Received signal strength prediction based multi-connectivity handover scheme for ultra-dense networks. In 2018 24th Asia-Pacific Conference on Communications (APCC) Nov 12 (pp. 233–238). IEEE. (2018).
37. Lu Y, Zhang C, Chen D, Zhang W, Xiong K. Handover Enhancement in High-Speed Railway 5G Networks: A LSTM-based Prediction Method. In 2022 13th International Conference on Computing Communication and Networking Technologies (ICCCNT) Oct 3 (pp. 1–6). IEEE. (2022).
38. Kaur, G., Goyal, R. K. & Mehta, R. An efficient handover mechanism for 5G networks using hybridization of LSTM and SVM. *Multimedia Tools Appl.* **81**(26), 37057–37085 (2022).
39. Aljeri, N. & Boukerche, A. A two-tier machine learning-based handover management scheme for intelligent vehicular networks. *Ad. Hoc. Netw.* **1**(94), 101930 (2019).
40. Aljeri N, Boukerche A. An efficient handover trigger scheme for vehicular networks using recurrent neural networks. In Proceedings of the 15th ACM International Symposium on QoS and Security for Wireless and Mobile Networks Nov 25 (pp. 85–91). (2019).
41. Sun G, Zemuy GT, Xiong K. Dynamic reservation and deep reinforcement learning based autonomous resource management for wireless virtual networks. In 2018 IEEE 37th International Performance Computing and Communications Conference (IPCCC) Nov 17 (pp. 1–4). IEEE. (2018).
42. AlQerm, I. & Shihada, B. Energy efficient traffic offloading in multi-tier heterogeneous 5G networks using intuitive online reinforcement learning. *IEEE Trans. Green Commun. Networks.* **3**(3), 691–702 (2019).
43. Puspita RH, Shah SD, Lee GM, Roh BH, Oh J, Kang S. Reinforcement learning based 5G enabled cognitive radio networks. In 2019 International Conference on Information and Communication Technology Convergence (ICTC) Oct 16 (pp. 555–558). IEEE. (2019).
44. Marzari L, Pore A, Dall'Alba D, Aragon-Camarasa G, Farinelli A, Fiorini P. Towards hierarchical task decomposition using deep reinforcement learning for pick and place subtasks. In 2021 20th International Conference on Advanced Robotics (ICAR) Dec 6 (pp. 640–645). IEEE. (2021).
45. Li Y. Deep reinforcement learning: An overview. arXiv preprint [arXiv:1701.07274](https://arxiv.org/abs/1701.07274). Jan 25. (2017).
46. Pugliese, R., Regondi, S. & Marini, R. Machine learning-based approach: Global trends, research directions, and regulatory standpoints. *Data Sci. Manag.* **1**(4), 19–29 (2021).
47. Yan, L. et al. Machine learning-based handovers for sub-6 GHz and mmWave integrated vehicular networks. *IEEE Trans. Wireless Commun.* **18**(10), 4873–4885 (2019).
48. Mahfouz, S., Mourad-Chehade, F., Honeine, P., Farah, J. & Snoussi, H. Kernel-based machine learning using radio-fingerprints for localization in wsns. *IEEE Trans. Aerosp. Electron. Syst.* **51**(2), 1324–1336 (2015).
49. Kushki, A., Plataniotis, K. N. & Venetsanopoulos, A. N. Kernel-based positioning in wireless local area networks. *IEEE Trans. Mob. Comput.* **6**(6), 689–705 (2007).
50. Bang, J. H., Oh, S., Kang, K. & Cho, Y. J. A Bayesian regression based LTE-R handover decision algorithm for high-speed railway systems. *IEEE Trans. Veh. Technol.* **68**(10), 10160–10173 (2019).
51. Chen, Y., Niu, K. & Wang, Z. Adaptive handover algorithm for LTE-R system in high-speed railway scenario. *IEEE Access.* **19**(9), 59540–59547 (2021).
52. Wu J, Liu J, Huang Z, Zheng S. Dynamic fuzzy Q-learning for handover parameters optimization in 5G multi-tier networks. In 2015 international conference on wireless communications & signal processing (WCSP) Oct 15 (pp. 1–5). IEEE. (2015).
53. Muñoz, P., Barco, R. & de la Bandera, I. On the potential of handover parameter optimization for self-organizing networks. *IEEE Trans. Veh. Technol.* **62**(5), 1895–1905 (2013).
54. Adadi, A. A survey on data-efficient algorithms in big data era. *J. Big Data.* **8**(1), 24 (2021).
55. Chen, Y. *Thinning algorithms for simulating point processes* (Florida State University, 2016).
56. Carrington, A. M. et al. Deep ROC analysis and AUC as balanced average accuracy, for improved classifier selection, audit and explanation. *IEEE Trans. Pattern Anal. Mach. Intell.* **45**(1), 329–341 (2022).
57. Shaked M, Shanthikumar JG. Stochastic orders. New York, NY: Springer New York; Apr 3. (2007).
58. Cali, C. & Longobardi, M. Some mathematical properties of the ROC curve and their applications. *Ricerche mat.* **64**, 391–402 (2015).
59. Khorshedd, M. S. & Al-Thubaity, A. O. Comparative evaluation of text classification techniques using a large diverse Arabic dataset. *Lang. Resour. Eval.* **47**, 513–538 (2013).
60. Nguyen, Q. H. et al. Influence of data splitting on performance of machine learning models in prediction of shear strength of soil. *Math. Probl. Eng.* **5**(2021), 1–5 (2021).
61. Leema, N., Nehemiah, H. K. & Kannan, A. Neural network classifier optimization using differential evolution with global information and back propagation algorithm for clinical datasets. *Appl. Soft Comput.* **1**(49), 834–844 (2016).
62. Dao, D. V. et al. A sensitivity and robustness analysis of GPR and ANN for high-performance concrete compressive strength prediction using a Monte Carlo simulation. *Sustainability.* **12**(3), 830 (2020).
63. Mismar, F. B., AlAmmouri, A., Alkhateeb, A., Andrews, J. G. & Evans, B. L. Deep learning predictive band switching in wireless networks. *IEEE Trans. Wireless Commun.* **20**(1), 96–109 (2020).

64. Va, V., Choi, J. & Heath, R. W. The impact of beamwidth on temporal channel variation in vehicular channels and its implications. *IEEE Trans. Veh. Technol.* **66**(6), 5014–5029 (2016).
65. Kim MS, Lee TS, Im TH, Ko HL. The analysis of coherence bandwidth and coherence time for underwater channel environments using experimental data in the West sea, Korea. In OCEANS 2016-Shanghai Apr 10 (pp. 1–4). IEEE. (2016).
66. Va V, Heath RW. Basic relationship between channel coherence time and beamwidth in vehicular channels. In 2015 IEEE 82nd Vehicular Technology Conference (VTC2015-Fall) Sep 6 (pp. 1–5). IEEE. (2015).
67. Sorrentino, A., Ferrara, G. & Migliaccio, M. On the coherence time control of a continuous mode stirred reverberating chamber. *IEEE Trans. Antennas Propag.* **57**(10), 3372–3374 (2009).
68. Majid, S. I. et al. Using an Efficient Technique Based on Dynamic Learning Period for Improving Delay in AI-Based Handover. *Mobile Inf. Sys.* **2021**(1), 2775278 (2021).
69. Manalastas, M., Farooq, M. U., Zaidi, S. M., Abu-Dayya, A. & Imran, A. A data-driven framework for inter-frequency handover failure prediction and mitigation. *IEEE Trans. Veh. Technol.* **71**(6), 6158–6172 (2022).
70. Mbulwa, A. I., Yew, H. T., Chekima, A. & Dargham, J. A. Self-optimization of handover control parameters for 5G wireless networks and beyond. *IEEE Access.* **22**(12), 6117–6135 (2023).
71. Sun K, Han Q, Yang Z, Huang W, Zhang H, Leung VC. Proactive Handover Type Prediction and Parameter Optimization Based on Machine Learning. *IEEE Transactions on Wireless Communications.* Jan 31. (2025).

Acknowledgements

This work is partially supported by National Science Centre of Poland Grant 2020/37/B/ST7/01448 and by the Icelandic Research Fund Grant 2410297.

Author contributions

"Conceptualization, S.I.M and Sh.I.M and S.Kh (Salahuddin Khan); methodology, A.A and N.G and S.K and H.A and Sh.K (Shahid Khan); formal analysis, S.I.M and Sh.I.M and Sh.K; data management, H.A and N.G; writing—original draft, S.I.M and Sh.K; project administration, A.A and S.K and S.Kh; funding acquisition, S.K. All authors have read and agreed to the published version of the manuscript."

Funding

National Science center of Poland grant,2020/37/B/ST7/01448,Icelandic Research Fund Grant,2410297

Declarations

Competing interests

The authors declare no competing interests.

Additional information

Correspondence and requests for materials should be addressed to S.K. or S.K.

Reprints and permissions information is available at www.nature.com/reprints.

Publisher's note Springer Nature remains neutral with regard to jurisdictional claims in published maps and institutional affiliations.

Open Access This article is licensed under a Creative Commons Attribution-NonCommercial-NoDerivatives 4.0 International License, which permits any non-commercial use, sharing, distribution and reproduction in any medium or format, as long as you give appropriate credit to the original author(s) and the source, provide a link to the Creative Commons licence, and indicate if you modified the licensed material. You do not have permission under this licence to share adapted material derived from this article or parts of it. The images or other third party material in this article are included in the article's Creative Commons licence, unless indicated otherwise in a credit line to the material. If material is not included in the article's Creative Commons licence and your intended use is not permitted by statutory regulation or exceeds the permitted use, you will need to obtain permission directly from the copyright holder. To view a copy of this licence, visit <http://creativecommons.org/licenses/by-nc-nd/4.0/>.

© The Author(s) 2025